IOP Publishing Journal of Physics D: Applied Physics
J. Phys. D: Appl. Phys. **55** (2022) 223001 (13pp) https://doi.org/10.1088/1361-6463/ac4d47

Topical Review

Flexible thermoelectric films based on interconnected magnetic nanowire networks

Tristan da Câmara Santa Clara Gomes*, Nicolas Marchal, Flavio Abreu Araujo and Luc Piraux*

Institute of Condensed Matter and Nanosciences, Université Catholique de Louvain, Place Croix du Sud 1, 1348 Louvain-la-Neuve, Belgium

E-mail: tristan.dacamara@uclouvain.be and luc.piraux@uclouvain.be

Received 4 October 2021, revised 10 December 2021
Accepted for publication 20 January 2022
Published 3 February 2022

Abstract

Recently, there has been increasing interest in the fabrication of flexible thermoelectric devices capable of cooling or recovering waste heat from hot surfaces with complex geometries. This paper reviews recent developments on three-dimensional networks of interconnected ferromagnetic nanowires, which offer new perspectives for the fabrication of flexible thermoelectric modules. The nanowire arrays are fabricated by direct electrodeposition into the crossed nanopores of polymeric templates. This low-cost, easy and reliable method allows control over the geometry, composition and morphology of the nanowire array. Here we report measured thermoelectric characteristics as a function of temperature and magnetic field of nanowire networks formed from pure metals (Co, Fe, Ni), alloys (NiCo, NiFe and NiCr) and FM/Cu multilayers (with FM = Co, $Co_{50}Ni_{50}$ and $Ni_{80}Fe_{20}$). Homogeneous nanowire arrays have high thermoelectric power factors, almost as high as their bulk constituents, and allow for positive and negative Seebeck coefficient values. These high thermoelectric power factors are essentially maintained in multilayer nanowires which also exhibit high magnetic modulability of electrical resistivity and Seebeck coefficient. This has been exploited in newly designed flexible thermoelectric switches that allow switching from an 'off' state with zero thermoelectric output voltage to an 'on' state that can be easily measured by applying or removing a magnetic field. Overall, these results are a first step towards the development of flexible thermoelectric modules that use waste heat to power thermally activated sensors and logic devices.

Keywords: 3D nanowire networks, thermoelectricity, template assisted electrodeposition, spin-dependent thermoelectricity, thermoelectric switch

(Some figures may appear in colour only in the online journal)

* Authors to whom any correspondence should be addressed.

1. Introduction

Nanowire structures have been widely studied in the field of thermoelectric conversion, notably because of their potential as thermoelectric materials with improved figure of merit ($ZT = S^2\sigma/\kappa$, with S, σ and κ, the Seebeck coefficient, electrical and thermal conductivities of the material, respectively), which is the physical parameter that accounts for the electrical-thermal energy conversion efficiency of thermoelectric materials. Improved ZT in nanowire-based materials have mainly been achieved by decreasing the thermal conductivity due to enhanced phonon scattering without substantial degradation of the electrical conductivity [1–5]. Notably, Bi and Bi-based alloys nanowires (NWs) have been widely studied as potential high-ZT materials, although several challenges such as achieving adequate crystalline structure have mitigated the thermoelectric performances [6–10]. Highly-doped silicon NWs have also raised interest due to their nanoscopic dimensions, their complementarity to CMOS, and their improved ZT for both *p*-type (positive thermopower) and *n*-type (negative thermopower) doping compared to bulk silicon values [4, 5].

On the other hand, 3d ferromagnetic metals exhibit relatively large thermopowers, which can be ascribed to the pronounced structure of the d-band and the high energy derivative of the density of states at the Fermi level as well as to the substantial magnon-drag contribution to the thermoelectric power within a wide temperature range [11–13]. In particular, ferromagnets have been found to have high potential for the active Peltier cooling of hotspots due to the combination of a high power factor ($PF = S^2/\rho$, with ρ the electrical resistivity) and high thermal conductivity [14, 15]. The power factor is the physical parameter that relates to the output power density of a thermoelectric material. It is interesting to note that the largest PF at room temperature (RT) is found for pure Co ($PF \approx 15\ mW\,K^{-2}\,m^{-1}$ [13]). In this context, arrays made of ferromagnetic NWs have also been studied, showing that the advantageous thermoelectric properties are essentially preserved in such nanostructures [16–18].

Furthermore, multilayer NWs made by alternating ferromagnetic (FM) and normal metal (NM) layers allows for large spin-dependent Seebeck and Peltier effects, which have been measured in single NW [19], arrays of parallel NWs [20] or three-dimensional (3D) NW networks [21–23]. In these FM/NM multilayers, magnetic control of the thermoelectric energy conversion can be achieved through the spin-dependent Seebeck and Peltier effects [24]. These effects result from a large magnetic field variation of the thermopower similar to the giant magnetoresistance (GMR) effect in FM/NM multilayers, especially when measurements are made in the current-perpendicular-to-plane (CPP) configuration. In the limit of no-spin relaxation, most of the GMR and spin-dependent thermoelectric effects can be understood using a simple two-current series resistor model where 'up' and 'down' charge carriers are propagating independently in two spin channels with large spin asymmetries in the electrical resistivity and the thermopower [25–28].

In addition, there has been growing interest in nanocomposites formed by inorganic NWs embedded in organic hosts for their potentials as efficient thermoelectric materials that are light-weight, flexible, bendable and shapeable [16, 29]. These key advantages allow the thermoelectric devices to harness thermal energy of hot surfaces with complex geometries or even the human body and offer innovative perspectives in a sustainable development context and the development of miniature, lightweight and functional portable electronic devices [30–32]. However, to date, flexible thermoelectric generators made of conducting polymers and their corresponding nanocomposites exhibit much lower properties compared to inorganic thermoelectric materials [33, 34].

The recent development of three-dimensional networks made of interconnected NWs has raised new perspectives in the field of thermoelectric nanowires. Indeed, this novel nanoarchitecture has several key advantages over parallel NWs arrays, such as the robustness of the NW array and the suitability of the structure for electrical and thermoelectric measurements in the plane of the film containing the NW array [21, 22, 29]. In contrast to parallel arrays of NWs where the thermal and electrical current can only be applied along the direction parallel to the NW axis (i.e. perpendicular to the NW-based films whose thickness is a few tens of μm maximum), the 3D NW structure allows to applied thermal and electrical current in the macroscopic in-plane direction, while the current is locally restricted along the NW axis direction, leading to a potential for much larger temperature gradient at the edges of the samples and increased thermoelectric output signal. These 3D NW networks can be embedded within organic membranes so that the NWs—membrane composite has flexible properties, while the template also protect the NWs from oxidation. As a result, interconnected NW networks are very promising for applications in the field of flexible thermoelectricity [21, 22, 29].

In this paper, interconnected nanowire networks, either made of homogeneous FM materials, e.g. pure metals (Co, Ni, Fe) and NiCo, NiFe and NiCr alloys, or made of FM/Cu (with FM = Co, $Co_{50}Ni_{50}$ or $Ni_{80}Fe_{20}$) multilayers, have been grown by electrodeposition into 3D porous polycarbonate templates, and their thermoelectric and magneto-thermoelectric properties were measured. In addition, thermocouples made from FM/Cu multilayer CNWs and from homogeneous FM CNWs were fabricated. By fine-tuning the material composition of the two legs, magnetically activated thermoelectric switches were obtained. The ability to switch from a zero thermoelectric output voltage to a voltage of several tens of μV following the application or removal of an external magnetic field was demonstrated.

2. Materials and methods

2.1. Fabrication of crossed nanowires for flexible thermoelectric films

The template-assisted electrodeposition technique has proven to be the most efficient method for the fabrication of 3D NW arrays with controlled size, geometry, composition and surface morphology [35]. In this approach, the crossed nanowire (CNW) networks simply replicate the porous templates [35].

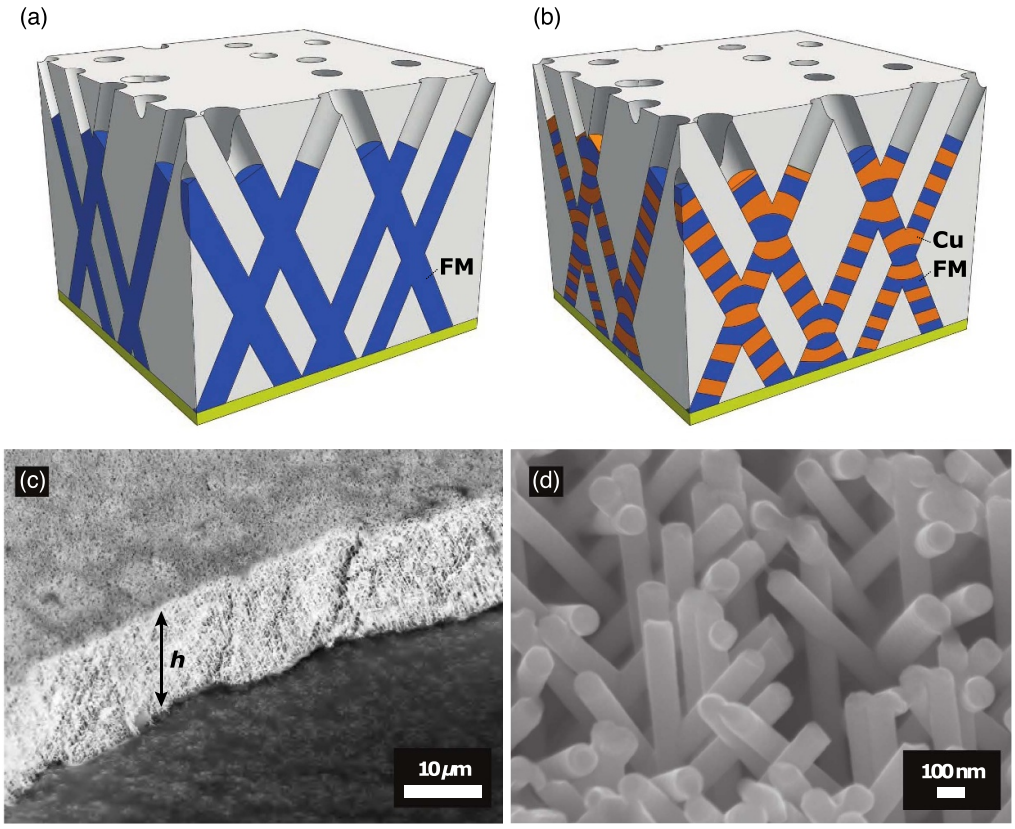

Figure 1. (a), (b) Schematics of crossed nanowire networks made of homogeneous material (a) and ferromagnetic (FM)/Cu multilayers (b). (c), (d) Images of self-supported interconnected nanowire networks obtained by scanning electron microscopy. (c) Low-magnification image showing the 50° tilted view of the macroscopic NW network film. (d) Higher magnification image of the sample in (c).

Track-etched polymer membranes with cylindrical crossed nanopores are obtained by sequential irradiation of a polycarbonate (PC) film with energetic heavy ions at different angles of incidence, followed by selective chemical etching of the ion tracks in the polymer film [36–38]. In addition to the precise control the geometrical parameters of the 3D porous structure and the level of porosity, this approach allows for large surface area membranes.

In this work, the 3D porous templates are fabricated by exposing 22 μm thick PC films to several irradiation steps with Ar^{9+} ions. The polymer film was first subjected to an irradiation step with incident angles of $+25°$ and $-25°$ with respect to the normal of the PC film surface. Next, for the second irradiation step the film was rotated in the plane by 90° and re-exposed to the same irradiation flux to finally form cylindrical crossed NWs with mean diameter of 80 nm and porosity of about 3%. Then, the PC templates are coated on one side with a metallic Cr/Au bilayer to serve as cathode during the electrodeposition of NWs networks. The thickness of the thin adhesion layer of Cr is set to 3 nm, while the thickness of the Au layer is set to 400 nm to ensure complete and uniform pore coverage prior to the electrodeposition process.

Homogeneous CNWs made of ferromagnetic metals and alloys, as schematically shown in figure 1(a), are grown from homemade electrolyte with adequate metallic ions composition by electrodeposition in potentiostatic mode at RT [39, 40]. In this study, CNWs made of pure FM (Ni, Co, Fe) have been fabricated, as well as CNWs made of NiCo, NiFe and NiCr alloys. By adjusting the ion composition and the potential, the alloying composition can be precisely controlled [23, 40–43]. Moreover, the technique has been proved very versatile, allowing to grow 3D crossed ferromagnetic metallic nanotubes [43, 44] or crossed multilayer NWs where ferromagnetic layers (Co, $Co_{50}Ni_{50}$ and $Ni_{80}Fe_{20}$) and Cu layers are stacked along the NWs axis, as schematically shown in figure 1(b) [21–23, 45, 46]. These networks can be grown with desired shape and size to meet requirements of various practical applications.

Figures 1(c) and (d) show images of self-supported 3D CNW networks obtained by electron microscopy after the complete removal of the PC template and metallic cathode. The low-magnification image on figure 1(c) attests for the dense and robust structure made of 3D interconnected NWs. Figure 1(d) at larger magnification shows the interconnected NW structure.

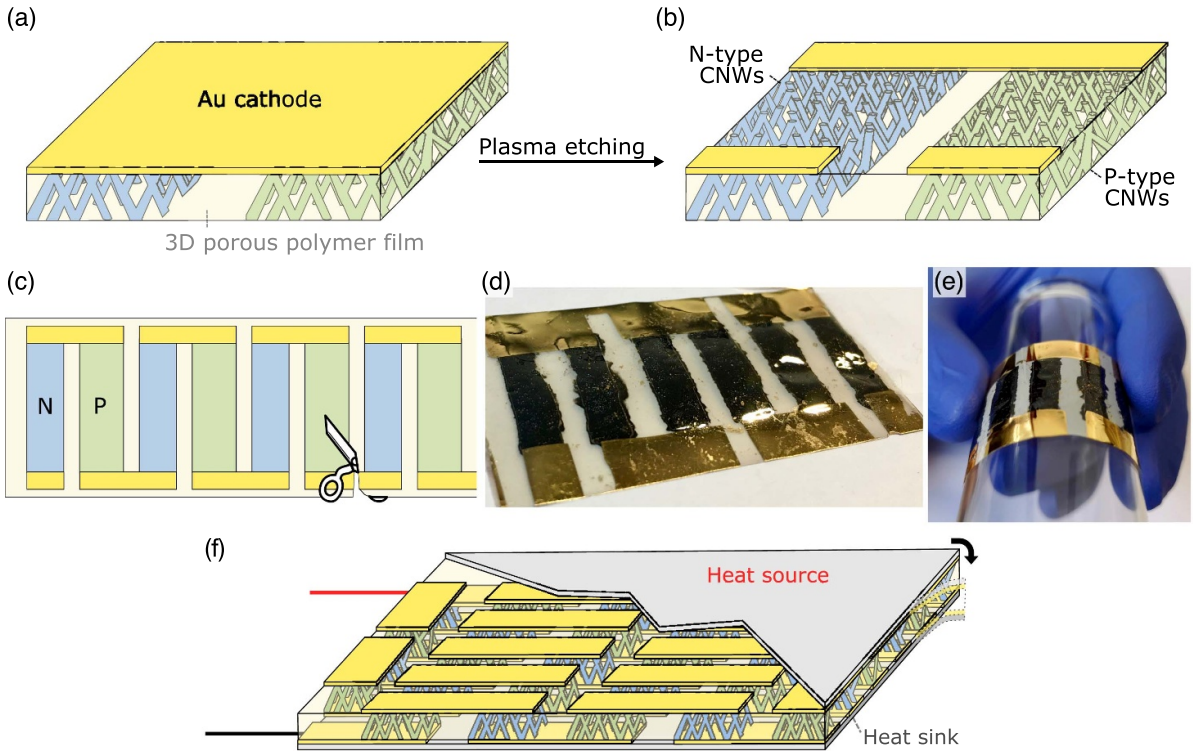

Figure 2. Fabrication technique of planar and flexible thermoelectric devices based on 3D nanowire networks. (a) *N*-type and *P*-type nanowire arrays are fabricated by two successive electrodeposition steps from the gold cathode into a 22 μm thick PC template. (b) An electrode design is obtained by plasma etching (under 5 mTorr of Ar plasma and 80 W) of the Au cathode to create a *p-n* thermoelectric junction. (c) Schematic of a planar thermoelectric device made of several 3D crossed nanowire *p-n* junctions. (d), (e) Pictures of a planar and flexible thermoelectric device with three *p-n* junctions made of crossed nanowire networks. The picture in (e) attests for the device flexibility and shapeability. (f) Schematic of a flexible thermoelectric module consisting of nanowire network-based thermocouples, as in (c), with a thermal gradient perpendicular to the film surface.

CNW networks are also appropriate for the fabrication of planar flexible thermoelectric thermocouples made of two dissimilar materials embedded within a single PC film [24]. The thermocouples are obtained by electrodepositing two adjacent NW networks from the Au cathode in the same PC template, with one branch made of *p*-type material, the other of *n*-type material, as shown in figure 2(a). Then, the Au cathode is locally removed by plasma etching to obtain the electrode design shown in figure 2(b). Moreover, these individual modules can be connected electrically in series and thermally in parallel to form more efficient thermoelectric devices, completely integrated within a flexible PC template, as shown in figure 2(c). Figure 2(d) shows a picture of a thermoelectric module composed of three CNW-based thermocouples. Figure 2(e) highlights the flexibility and shapeability of the device, which can be used to harness heat from hot surface with complex geometries or cool down electronic device with complex shapes [24]. It should be noted that the same fabrication technique can be easily adapted to fabricate flexible thermoelectric modules exploiting temperature differences that occur along the film normal (see figure 2(f)) [24]. This alternative configuration, combined with the miniaturization of both the electrodeposition process and the electrode patterning by plasma etching, allows the integration of a large number of thermocouples while limiting the lateral dimensions and the recovery of waste heat from complex shaped surfaces.

2.2. Experimental set-ups for electric and thermoelectric measurements

The growth of 3D ferromagnetic metal NW networks within PC template allows to obtain flexible thermoelectric materials without degrading the excellent thermoelectric and electrical transport properties of the constituting ferromagnetic metals [23, 29, 42]. The Seebeck coefficient and electrical resistivity for various homogeneous CNW networks made of various FM metals and alloys deposited into 22 μm thick PC template were measured using the experimental set-up reported in figures 3(a) and (b). First, a two-probe electrode design is obtained by local removing of the Cr/Au cathode using plasma etching, as described in [21, 29, 39]. The etched area, which corresponds to the area of the NW network that is measured, is about 2 mm long and 2 mm large. Because of the low thermal/electrical contact resistance between the Cr/Au cathode and the FM CNWs, this configuration is suitable for electrical and thermoelectric measurements. In addition, in order to obtain large and easily measurable signals, measurements are made with the thermal/electrical current applied globally along the macroscopic in-plane (IP) direction of the CNW networks while ensuring small-scale heat and charge flows along the NW axis. This is because the thermal conductivity of the electrically insulating PC host is much smaller than that of the metallic NWs. For thermoelectric measurements,

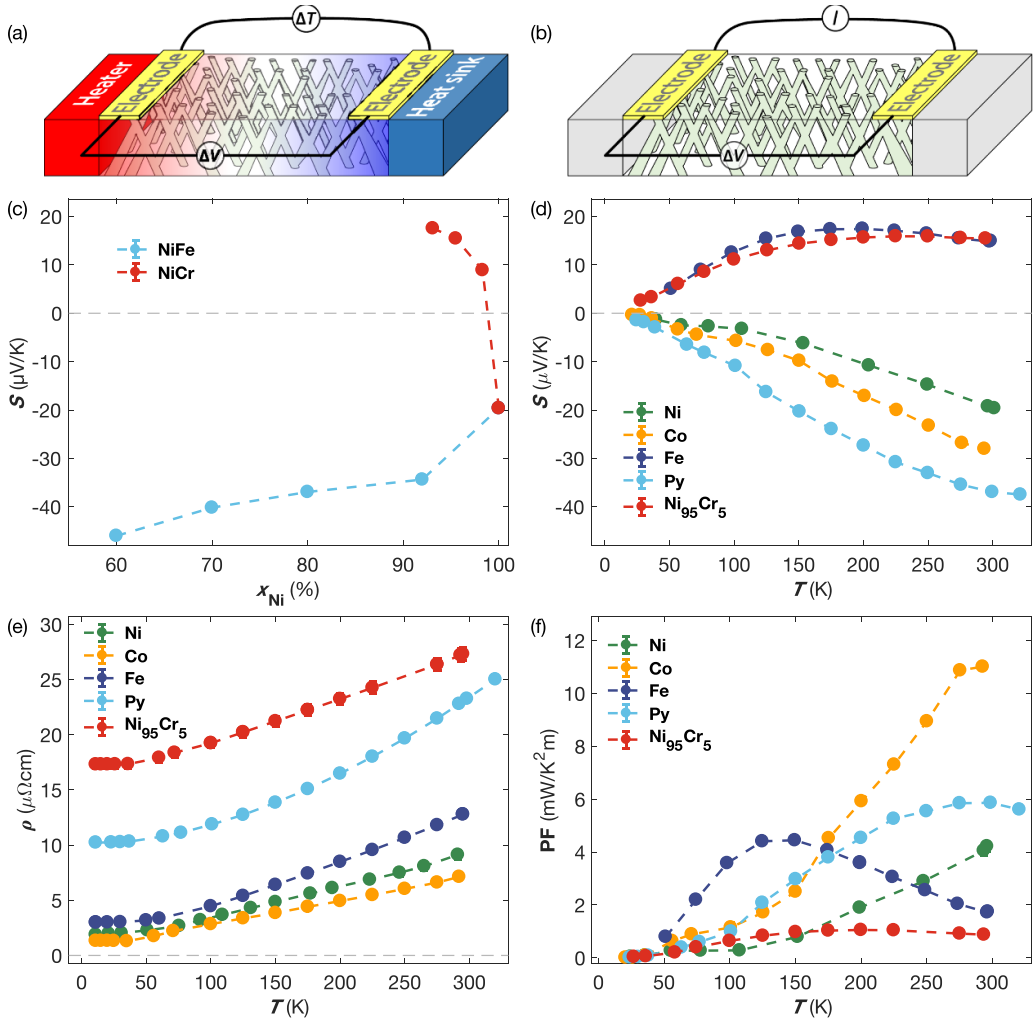

Figure 3. (a), (b) Device configuration for measurements of the Seebeck coefficient and the resistance of a 3D crossed nanowire networks. (a) Heat flow is generated by a resistive element, and a thermoelectric voltage ΔV is created by the temperature difference ΔT. (b) The voltage differential ΔV induced by the injected current I between the two metallic electrodes is measured while the two electrodes are maintained at the same constant temperature. (c) Seebeck coefficient as a function of the Ni content x_{Ni} for crossed nanowire networks made of NiFe and NiCr alloys. (d)–(f) Temperature dependencies of (d) the Seebeck coefficient S, (e) the resistivity ρ and (f) the power factor PF $= S^2/\rho$ of 3D crossed nanowire networks made of various ferromagnetic metals and alloys.

a resistive heater is connected to one electrode as depicted in figure 3(a) while the other electrode is connected to a heat sink maintained at constant temperature, giving rise to a thermal current through the CNW network that is measured using a type E differential thermocouple while the voltage is measured using thin chromel P wires (see [21] for details). A typical temperature difference of 1 K was used in the measurements. For electrical measurements, the two electrodes are kept at the same temperature while a direct current is injected through the CNW network generating the measured voltage. All contacts between leads and the Cr/Au electrodes are made using silver paint. Note that the measurements performed with a two-probe and a four-probe configuration, the latter allowing to remove the contact resistance from the measurement, provide identical resistance values because the electrical resistance of the network (from few Ω to few kΩ) is much larger than the ones attributed to the corresponding leads and contacts to the sample [39]. These thermoelectric and electrical measurements were performed under vacuum in a temperature range of 15 K–320 K and an external magnetic field was swept between ±10 kOe in the IP direction of the network for magneto-transport measurements.

3. Results

3.1. Thermoelectric properties of homogeneous nanowires

Table 1 provides the RT values for the Seebeck coefficient S of various FM CNW networks at zero magnetic field. As seen, the high Seebeck coefficients of ferromagnetic metals are preserved in the electrodeposited NW structures [29]. In addition, it is possible to make FM CNWs with Seebeck coefficient of opposite signs, allowing the fabrication of *p*-*n* thermocouples, as shown schematically in figure 2. The electrical resistivity ρ of FM CNWs was extracted from the resistance measurements at RT and at 15 K assuming that the

Table 1. Room-temperature Seebeck coefficient S, resistivity ρ, power factor PF and figure of merit ZT for several homogeneous and multilayer crossed nanowire networks. The grey color highlights the p-type thermoelectric materials. The values are reported at zero external magnetic field for the homogeneous networks and in the saturated state for the multilayer nanowire networks.

	S (μV K^{-1})	ρ ($\mu\Omega$cm)	PF (mW K^{-2} m^{-1})	ZT
Co	−28.0	7.1	11.0	3.2×10^{-2}
Fe	+15.0	12.8	1.8	9.1×10^{-3}
Ni	−19.6	9.1	4.2	1.6×10^{-2}
$Ni_{90}Fe_{10}$	−34.4	18.6	6.3	4.8×10^{-2}
$Ni_{80}Fe_{20}$	−36.9	25.0	5.4	5.6×10^{-2}
$Ni_{70}Fe_{30}$	−40.2	32.5	5.0	6.6×10^{-2}
$Ni_{60}Fe_{40}$	−46.0	42.4	5.0	8.6×10^{-2}
$Ni_{96}Cr_4$	+15.5	27.3	0.9	9.8×10^{-3}
Co/Cu	−19.9	8.7	4.6	1.6×10^{-2}
$Co_{50}Ni_{50}$/Cu	−21.6	10.2	4.6	1.9×10^{-2}
$Ni_{80}Fe_{20}$/Cu	−24.8	15.3	4.0	2.5×10^{-2}

Matthiesen's rule holds and that the ideal resistivity at RT is the same as for FM bulk material (see [29] for details). It has indeed been previously pointed out that for a not too small NW diameter ($\geqslant$40 nm), thermally induced scattering effects are independent of sample dimensions, nanostructuring and defect concentration [47]. The RT electrical resistivity values, provided in table 1, are only slightly larger to that of the corresponding bulk FM materials. This is due to increased scattering of conduction electrons by defects in the electrodeposited nanostructured materials and additional surface scattering related to the nanoscale lateral dimensions of the NWs [29].

The thermoelectric properties of CNW networks were characterized by the power factor (PF $= S^2/\rho$) and the figure of merit ZT $= S^2T/\kappa\rho$. In the case of a metal, and assuming that the Wiedemann–Franz law applies ($\kappa\rho = L_0T$ with $L_0 = 2.45 \times 10^{-8}$ V^2 K^{-2}, the Lorentz number), the figure of merit is simply given by ZT $= S^2/L_0$. The values of PF and ZT at RT are reported in table 1 for various FM CNW networks. The PF values for CNWs were only slightly smaller than that of bulk FM materials, which can be ascribed to the slight increase in the residual electrical resistivity. PF $\approx$ 11 mW K^{-2} m^{-1} was found in Co CNW networks [42], which is close to the largest PF displayed by bulk Co at RT (PF $\approx$ 15 mW K^{-2} m^{-1} [13]) and about twice larger to that of widely used thermoelectric material bismuth-telluride (in the range 1–6 mW K^{-2} m^{-1} [48]). Although the investigated p-type CNWs show lower PFs than the investigated n-type CNWs, those PF values are at least one order of magnitude larger than the ones reported for flexible thermoelectric films based on optimized conducting polymers [34]. As a consequence, 3D CNW networks embedded into PC membrane are promising flexible materials for active cooling applications that require large PF and thermal conductivity [14, 15]. The ZT values at RT are found to be about one to two orders of magnitude smaller than those of state-of-the-art thermoelectric materials (current record value of ZT $= 1.86$ at 320 K in bismuth antimony telluride alloys [49]). However, it is comparable to those of thermocouple alloys (ZT $\approx 6 \times 10^{-2}$ and ZT $\approx 1.4 \times 10^{-2}$ in constantan and chromel, respectively) and can be used in applications for devices with low energy requirements where the heat supply comes from recovered waste heat.

The RT Seebeck coefficient of CNW networks made of FM alloys was found to be highly adjustable by changing the alloy composition. For example, the addition of Fe or Cr impurities in Ni CNWs can be used to modify the thermopower towards more negative or positive values [23, 42]. Figure 3(c) shows the RT Seebeck coefficient of NiFe and NiCr CNW networks depending on the composition of the alloy. As seen, the increase of Fe concentration leads to a monotonous increase of the magnitude of the negative thermopower up to -46.0 μV K^{-1} for 40% of Fe into Ni CNWs. In contrast, the addition of Cr impurity changes the sign of the thermopower, with Seebeck coefficient reaching $+17.5$ μV K^{-1} for 7% of Cr into Ni CNWs. This allows the Seebeck coefficient to be fine-tuned for the desired applications. However, the addition of Fe or Cr impurities also induces larger residual resistivity due to impurity scattering.

The temperature variation of the Seebeck coefficient S of various FM CNW networks was also measured in the range $T =$ 20–320 K, as reported in figure 3(d). As expected, the thermopower tends towards very low values at low temperatures. The temperature variations of S observed on the CNWs are globally similar to those of the corresponding bulk materials, except for the absence of of phonon-drag peaks in the thermopower resulting from the nanostructuring [12]. Figure 3(e) shows the temperature dependence of the electrical resistivity of FM CNWs, which exhibits metallic behavior. As expected, FM alloys lead to higher residual electrical resistivity, due to diffusion by impurities. For temperatures between 100 K and 300 K, the temperature variation is almost linear. The temperature variation of the thermoelectric power factor is reported in figure 3(f). It illustrates the large PF values of Co CNWs around RT, while Py and Ni also display relatively large PF. In contrast, the p-type samples have smaller PF around RT.

3.2. *Magneto-thermoelectric properties of multilayer nanowires*

Interconnected FM/Cu multilayer CNW networks have been found to combine large thermopower and large variation of their electrical and thermoelectrical properties under external magnetic fields [21–23, 29]. These nanostructures make it possible to measure giant magnetoresistance (GMR) responses and its analogue magneto-thermopower effect with the electrical/thermal current flowing perpendicularly to the plane of the layers in the individual NW segments (CPP configuration) and thus overall in the plane of the 3D CNW network film, as illustrated in figure 4(a) [43]. Interestingly, the Seebeck coefficient of 3D CNWs made of FM metals and alloys is only slightly reduced when stacking thin FM and Cu layers along the NW axis in 3D CNW networks [21–23]. Indeed, in the CPP

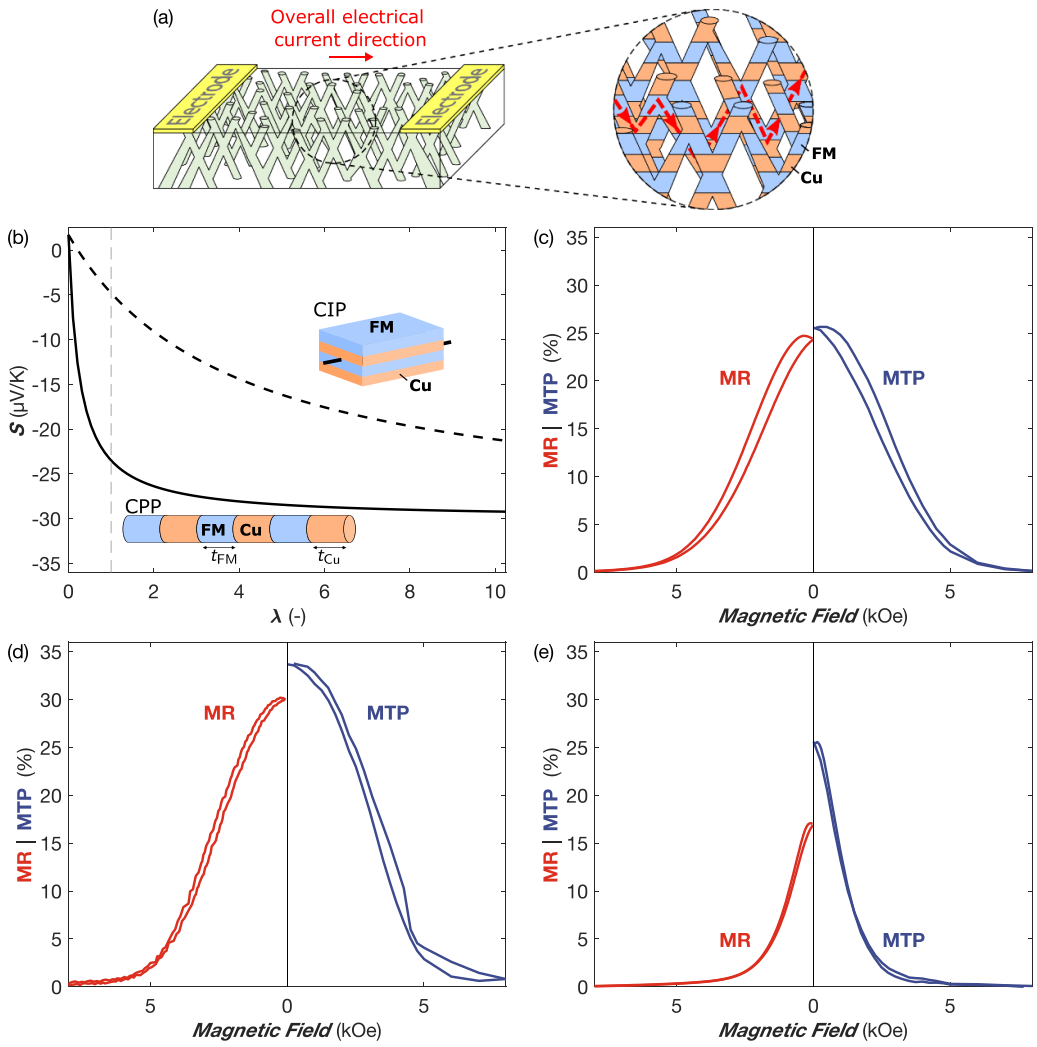

Figure 4. (a) Schematic of the giant magnetoresistance measurement in multilayer nanowire-based films, where the electrical transport takes place globally in the plane of the film while the architecture based on crossed nanowires ensures a CPP-type transport. (b) Calculated thermopowers for Co/Cu multilayers in the layer parallel (dash-dotted line—CIP) and perpendicular (solid line—CPP) directions as a function of the thickness ratio $\lambda = t_{Co}/t_{Cu}$, using equations (2) and (3) and the bulk values for S_{Co}, ρ_{Co}, S_{Cu} and ρ_{Cu}. The grey dashed line shows the values for $\lambda = 1$. The insets in (b) show FM/Cu multilayer stacks with CIP and CPP configurations. (c)–(e) Room-temperature variation of the electrical resistance (red, left) and Seebeck coefficient (blue, right) obtained by applying a magnetic field in the plane of (c) Co/Cu, (d) $Co_{50}Ni_{50}$/Cu, (e) $Ni_{80}Fe_{20}$/Cu crossed nanowire networks.

configuration, the Seebeck coefficient along the axial direction (perpendicular direction to the layers) can be calculated from the corresponding transport properties using Kirchhoff's rules [50] as

$$S_{\mathrm{CPP\ FM/Cu}} = \frac{S_{\mathrm{Cu}}\kappa_{\mathrm{FM}} + \lambda S_{\mathrm{FM}}\kappa_{\mathrm{Cu}}}{\lambda\kappa_{\mathrm{Cu}} + \kappa_{\mathrm{FM}}}, \tag{1}$$

where S_{FM}, S_{Cu} and κ_{FM}, κ_{Cu} represent the thermopower and the thermal conductivity of the FM and Cu, respectively, and $\lambda = t_{FM}/t_{Cu}$ the thickness ratio of FM and Cu layers. Because FM metals and alloys exhibit much larger Seebeck coefficient than Cu, and their thermal conductivity is expected to be smaller than that of Cu, using $S_{FM}\kappa_{Cu} \gg S_{Cu}\kappa_{FM}$ in equation (1) leads to $S_{\mathrm{CPP\ FM/Cu}} \approx S_{FM}$, for a thickness ratio λ not too small.

Moreover, assuming that the Wiedemann–Franz law holds for the Cu and FM, the thermopower in CPP configuration can also be written as

$$S_{\mathrm{CPP\ FM/Cu}} = \frac{S_{\mathrm{Cu}}\rho_{\mathrm{Cu}} + \lambda S_{\mathrm{FM}}\rho_{\mathrm{FM}}}{\lambda\rho_{\mathrm{FM}} + \rho_{\mathrm{Cu}}}, \tag{2}$$

with ρ_{FM} and ρ_{Cu} being the corresponding electrical resistivities. By comparison, the Seebeck coefficient of a planar FM/Cu multilayer stack in the direction parallel to the layers (CIP) is given by

$$S_{\mathrm{CIP\ FM/Cu}} = \frac{S_{\mathrm{Cu}}\rho_{\mathrm{FM}} + \lambda S_{\mathrm{FM}}\rho_{\mathrm{Cu}}}{\lambda\rho_{\mathrm{Cu}} + \rho_{\mathrm{FM}}}. \tag{3}$$

Figure 4(b) illustrates the contrasting behavior between the Seebeck coefficient in the CIP and CPP configurations for

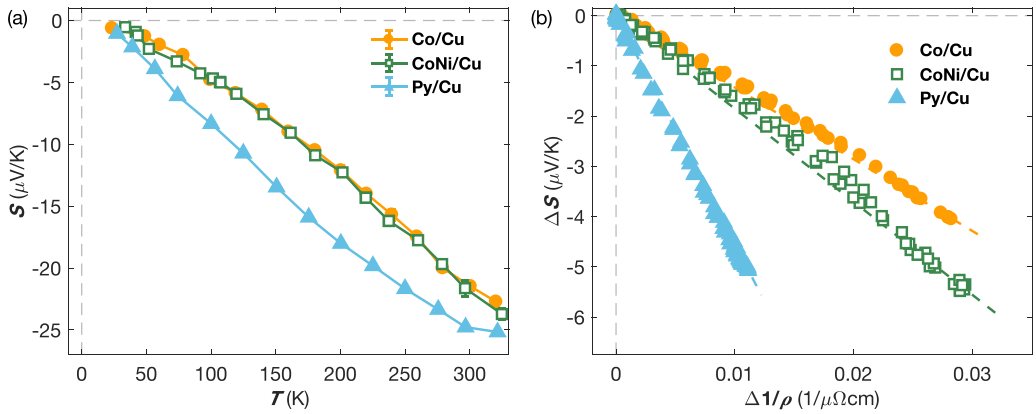

Figure 5. (a) Temperature variation of the Seebeck coefficient in the saturated state for Co/Cu, $Co_{50}Ni_{50}$/Cu and $Ni_{80}Fe_{20}$/Cu crossed nanowire networks. (b) Linear variation of $\Delta S(H) = S(H) - S_0$ vs. $\Delta(1/\rho(H)) = 1/\rho(H) - 1/\rho_0$ at room temperature, illustrating the Gorter–Nordheim characteristics for the Co/Cu, $Co_{50}Ni_{50}$/Cu and $Ni_{80}Fe_{20}$/Cu crossed nanowire networks. The dashed lines correspond to the theoretical relation shown in equation (4).

Co/Cu multilayers, using equations (2) and (3) and literature RT resistivity and thermopower values for bulk Co and Cu [51–55]. In the CPP configuration, the Seebeck coefficient of the Co/Cu multilayer system quickly converges toward the value of Co and already reaches about 80% of the thermopower of pure Co for $\lambda = 1$. In contrast, the CIP configuration requires very large values of λ to reach large thermopower values and only about 15% of the Seebeck coefficient of pure Co is reached for $\lambda = 1$. Note that in CIP system with dominant interface scattering, the thermopower becomes less sensitive to the Cu bulk resistance, which leads to larger S values [56]. Although the electrical resistivity and thermal conductivity values for multilayer NWs may vary significantly compared with their respective bulk constituents, the same trends in the contrasting behavior between the two configurations remain.

Figures 4(c)–(e) illustrate the large magnetoresistance (MR $= 1 - \rho_{sat}/\rho_0$, where ρ_0 and ρ_{sat} are the resistivities of the CNW network at zero magnetic field and at saturation magnetic field) and magneto-thermopower (MTP $= |1 - S_{sat}/S_0|$, where S_0 and S_{sat} are the Seebeck coefficients of the CNW network at zero magnetic field and at saturation magnetic field) effects obtained in Co/Cu (c), $Co_{50}Ni_{50}$/Cu (d) and Py/Cu (e) CNW networks. For the $Co_{50}Ni_{50}$/Cu system, the MR and MTP ratios reach 30.2% and 33.7%, respectively. The shapes of the MR and MTP curves were found to be very similar for all FM/Cu CNW networks [21–23, 46]. However, while the amplitudes of the MR and MTP effects are similar in Co/Cu and $Co_{50}Ni_{50}$/Cu networks [21, 22], very different magnitudes were found in Ni_xFe_{1-x}/Cu CNW networks, with the MTP/MR ratio ranging from ∼0.7 up to ∼7 [46]. Indeed, the amplitudes of the MR and MTP effect were found to arise from different spin asymmetry parameters for the resistivity and Seebeck coefficient and can take thus distinct values (see [29, 46] for details). Moreover, in contrast to the MR ratio, the MTP ratio can reach infinite value as the Seebeck coefficient of spin 'up' and spin 'down' electrons can have opposite sign [21, 29, 46]. It is interesting to note that the application of an external magnetic field simultaneously increases the thermopower magnitude and decreases the electrical resistivity of these FM/Cu CNWs, which are both advantageous for the thermoelectric output power.

Figure 5 presents additional evidences that the thermopower is dominated by electron diffusion over the whole temperature range investigated for the different multilayer CNW networks considered. As seen in figure 5(a), the Seebeck coefficient in the saturated state of all three samples decreases almost linearly with decreasing temperature, as expected from diffusive thermopower. The deviation from the linear regime in figure 5(a) can be ascribed to other possible contributions to the thermopower such as magnon-drag. Figure 5(b) shows linear variation of $\Delta S(H) = S(H) - S_0$ and $\Delta(1/\rho(H)) = 1/\rho(H) - 1/\rho_0$ at RT for Co/Cu $Co_{50}Ni_{50}$/Cu and Py/Cu CNW networks, which is also indicative of the dominance of diffusion thermopower. Indeed, starting from the Mott's formula for the diffusive thermopower, one can derive the following linear relation [56–58]:

$$\Delta S(H) = B\Delta(1/R(H)), \tag{4}$$

where $B = R_0\ R_{sat}(S_{sat} - S_0)/(R_0 - R_{sat})$. This expression is equivalent to the Gorter–Nordheim relation for diffusion thermopower in metals and alloys [11], and was well observed experimentally in all FM/Cu CNW networks studied in the temperature range of 15 K to 320 K [21–23, 29, 46].

Figures 6(a)–(c) shows the temperature dependence of the MR and MTP ratios for the Co/Cu (a), $Co_{50}Ni_{50}$/Cu (b) and Py/Cu (c) CNW networks. As seen, in all samples, the MR ratio shows a monotonic increase before reaching a plateau at low temperatures. This is expected because of the saturation of the resistivity at low temperatures and the vanishing of the spin mixing effect [21–23, 29, 46]. In contrast, the MTP ratio exhibits different behaviors depending on the material considered. Notably, large increase of the MTP ratio with respect to the corresponding MR ratio has been found in Ni and Ni_xFe_{1-x}/Cu CNW networks [23, 29, 46], as shown

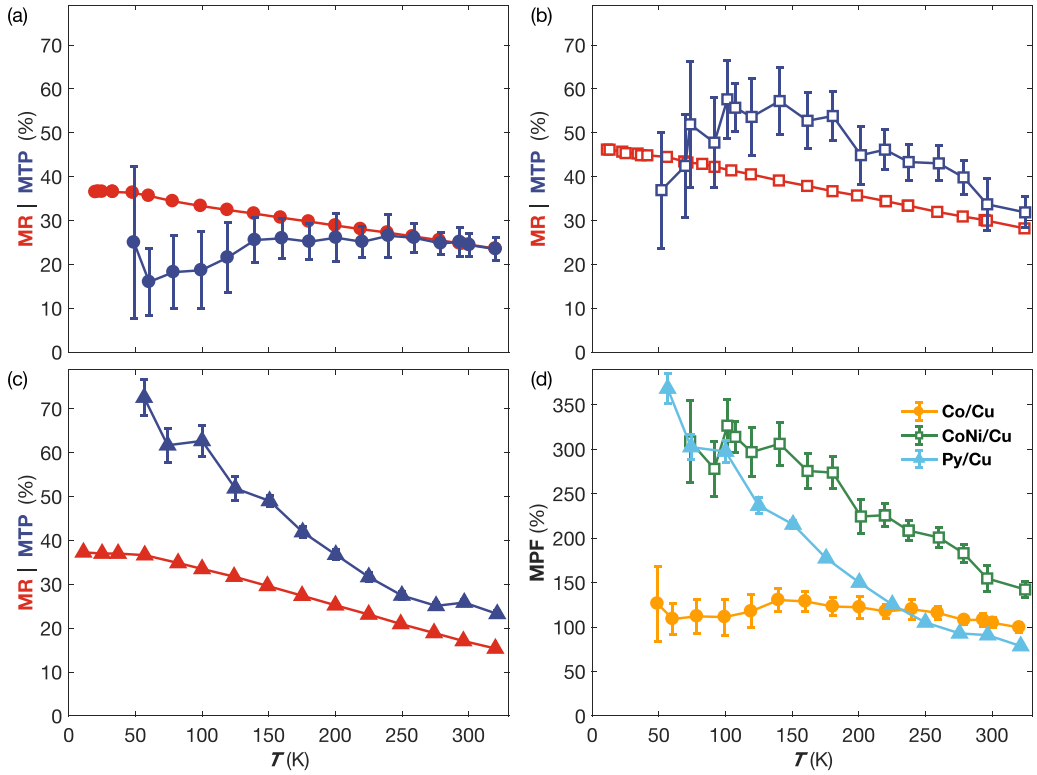

Figure 6. (a)–(c) Temperature variation of the magnetoresistance and magneto-thermopower ratios, MR and MTP, for (a) Co/Cu, (b) $Co_{50}Ni_{50}$/Cu and (c) $Ni_{80}Fe_{20}$/Cu crossed nanowire networks. The field is applied in the plane of NW network films. (d) Magneto-power factor ratio calculated as $\mathrm{MPF} = (1+\mathrm{MTP})^2/(1-\mathrm{MR}) - 1$ for the samples in (a)–(c).

in figure 6(c) for Py/Cu CNWs. The magneto-power factor ratio ($\mathrm{MPF} = 1 - \mathrm{PF}_{\mathrm{sat}}/\mathrm{PF}_0$) can be expressed as $\mathrm{MPF} = (1+\mathrm{MTP})^2/(1-\mathrm{MR}) - 1$ (taking $\mathrm{MR} = = 1 - \rho_{\mathrm{sat}}/\rho_0$ and $\mathrm{MTP} = |1 - S_{\mathrm{sat}}/S_0|$ as positive values). Figure 6(d) shows the MPF ratio for Co/Cu, $Co_{50}Ni_{50}$/Cu and Py/Cu CNW networks as a function of the temperature. Large RT MPF ratio of 111%, 155% and 92% were found for the Co/Cu, $Co_{50}Ni_{50}$/Cu and Py/Cu CNW networks, respectively, which arise from simultaneous increase of the Seebeck coefficient amplitude and decrease of the electrical resistivity with an applied magnetic field [21–23]. While the MPF ratio of the Co/Cu CNW network remains stable with decreasing temperature, the MPF values have been found to reach several hundreds of percent at low temperatures in $Co_{50}Ni_{50}$/Cu and Py/Cu CNW networks.

Regarding the thermoelectric performance of FM/Cu multilayer CNW networks, table 1 provides the Seebeck coefficient and electrical resistivity obtained at saturation field at RT for Co/Cu, $Co_{50}Ni_{50}$/Cu and Py/Cu CNW networks [21, 22]. From these values, the PF and ZT values were estimated and are also reported in table 1. As seen, PF values as high as 4.6 $\mathrm{mW\,K^{-2}\,m^{-1}}$ were obtained, which is only about twice smaller than that of Co CNWs, indicating that the excellent thermoelectric properties remain in FM/Cu multilayer CNWs. Similarly, the figure of merit of multilayer FM/Cu CNWs are only slightly smaller than that of their corresponding homogeneous FM CNW networks.

3.3. Magnetically activated switching in thermoelectric CNW devices

A new concept of flexible thermoelectric switch triggered by a magnetic field was developed using thermocouples composed of two dissimilar CNW networks embedded in a single PC template [24]. This device exploits the large magnetic variation of the Seebeck coefficient observed in FM/Cu CNWs which compose the first branch of the thermocouple, the other branch consisting of homogeneous FM CNWs with very small magneto-transport effects [29]. By appropriately selecting the materials of the FM/Cu and FM CNWs, it is possible to obtain flexible thermoelectric devices capable of switching from an 'off state' ($\Delta V = 0$, with ΔV the measured output voltage from the thermocouple) to an 'on state' (few tens of μV, easily measurable) at the saturation field of the FM/Cu CNWs, or vice versa at zero field. For instance, such switching devices were realized using thermocouples composed of a branch either made of $Co_{50}Ni_{50}$/Cu or Py/Cu CNWs and a branch made of Co_3Ni_{97} CNW network [24]. $Co_{50}Ni_{50}$/Cu and Py/Cu CNWs were selected because of the large values of $\Delta S = S_0 - S_{\mathrm{sat}}$, which reaches about 5.5 $\mu\mathrm{V\,K^{-1}}$ and 5.1 $\mu\mathrm{V\,K^{-1}}$ at RT, respectively. Then, the RT Seebeck coefficient of Co_3Ni_{97} CNWs was found to precisely match the one of $Co_{50}Ni_{50}$/Cu CNWs at saturation field, as well as the one of Py/Cu CNWs at zero field [24].

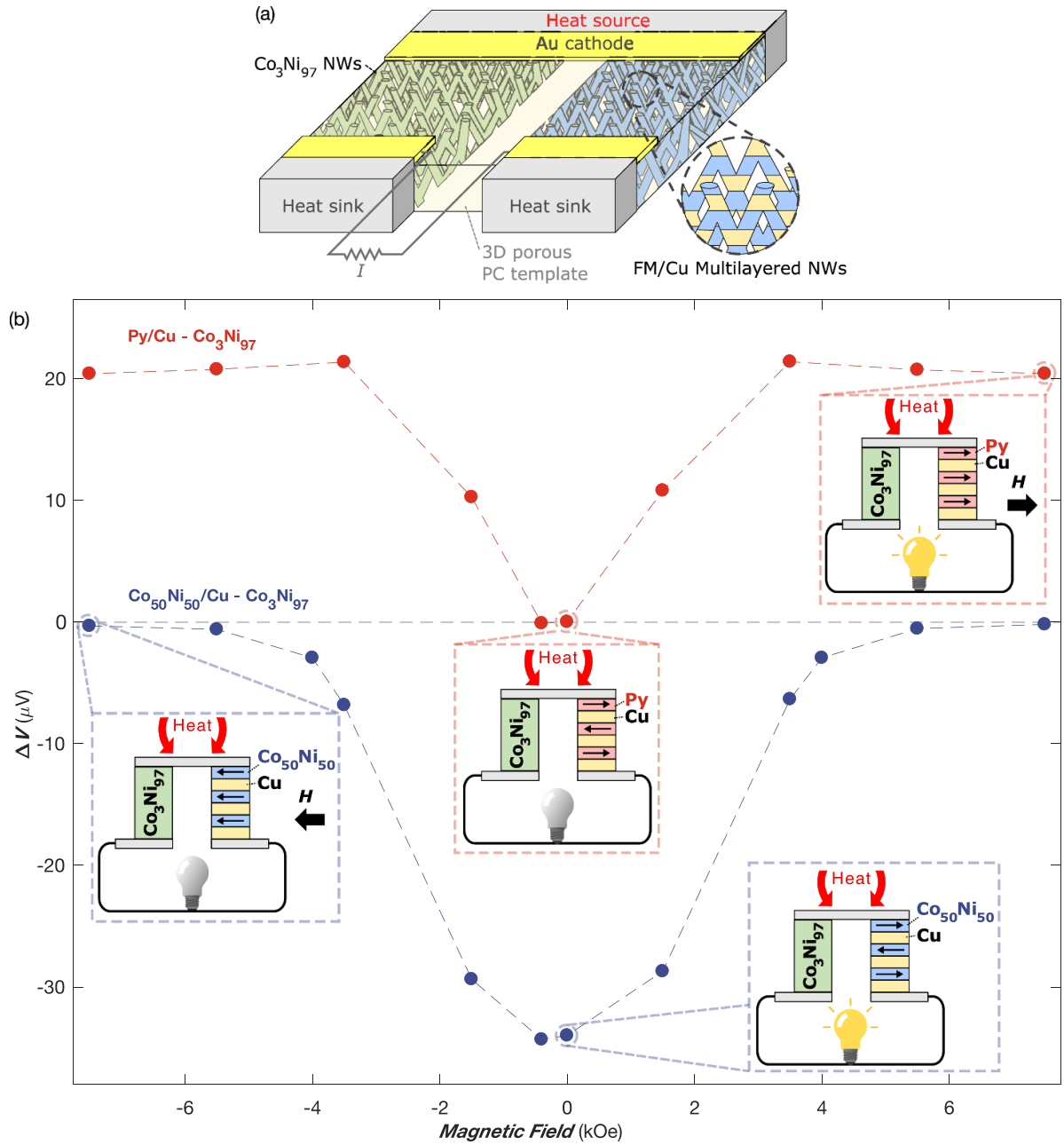

Figure 7. (a) Schematics of a magnetic switch thermoelectric thermocouple where the two crossed nanowire network legs are respectively composed of an homogeneous Co_3Ni_{97} and a FM/Cu multilayer structure with giant magneto-Seebeck effect (FM = Py or $Co_{50}Ni_{50}$). The thermopower voltage output generated by the heat flux flowing between the heat source and the heat sinks (maintained at desired temperature by a PID temperature controller) can be switched off or on by applying an external magnetic field that saturated the successive magnetization of the multilayer structure. (b) Variation of the voltage differential ΔV recorded at the junction edges for $\Delta T = 10$ K when sweeping a magnetic field from +7.5 kOe to −7.5 kOe in the plane of interconnected Py/Cu—Co_3Ni_{97} (red) and $Ni_{50}Co_{50}$/Cu—Co_3Ni_{97} (blue) nanowire network thermocouples at room temperature. The insets in (b) show schematics of the thermocouples 'on' and 'off' states.

The device is shown in figure 7(a). Two adjacent CNW networks are deposited within the flexible 3D porous template, one made of Co_3Ni_{97} CNWs and one of FM/Cu CNWs (with FM = $Co_{50}Ni_{50}$ or Py). Next, the Au cathode is removed locally by plasma etching to create the multi-electrode architecture. Thermoelectric measurements are made by placing the junction of the thermocouple in contact with the heat source while at the other extremity the two legs are thermally anchored to the heat sink, as shown in figure 7(a). For a homogeneous—multilayer CNWs thermocouples, the measured voltage ΔV of the NW-based thermocouple generated by a temperature gradient ΔT is given by [24]

$$\Delta V = \int_{T_0}^{T_0+\Delta T} (S_{\mathrm{HM}}(T) - S_{\mathrm{ML}}(T))\,\mathrm{d}T, \tag{5}$$

where T_0 is the heat-sink base temperature and S_{HM} and S_{ML} are the Seebeck coefficients of the homogeneous CNWs

and multilayer CNWs, respectively. Since the Seebeck coefficient of homogeneous CNWs shows a very small variation in magnetic field, the field dependence of the output voltage of thermocouples is mainly due to FM/Cu multilayer CNWs. Therefore, as seen in figure 7(b), the voltage differential ΔV obtained at the edges of a $Co_{50}Ni_{50}$/Cu CNWs—Co_3Ni_{97} CNWs thermocouple for a $\Delta T = 10$ K can be switched down from $\Delta V \approx -33$ μV at $H = 0$ to $\Delta V \approx 0$ by the application of a magnetic field that saturates the FM layer magnetization ($H = 7.5$ kOe). In contrast, the Py/Cu CNWs—Co_3Ni_{97} CNWs thermocouple shows $\Delta V \approx 0$ for $H = 0$, which can be increased to $\Delta V \approx +21$ μV at $H = 7.5$ kOe (see figure 7(b)). The thermoelectric switches were found to be robust, with no variation of the output voltage during different switching cycles obtained by sweeping the magnetic field between −8 kOe and 8 kOe [24].

Such thermoelectric switches have potential applications for logic operations devices powered by waste heat. From a practical point of view, the magnetic control of the magnitude and sign of the thermopower opens the route towards to the development of thermally activated sensors and logic devices exploiting the residual thermal energy from hot surfaces with complex geometries, or even from the human body. In addition, Onsager reciprocity between Peltier and Seebeck effects implies that a switchable Seebeck voltage results in a switchable Peltier heat flow. In a recent work, Adams *et al* [15] showed that a Peltier module can be seen as an active thermal switch that opens and closes under an activation current. Furthermore, it has been recently shown that multilayer NW arrays can magnetically control the Peltier thermal flux [21, 22]. Therefore, the flexible thermoelectric modules developed here can be used as thermal switches, offering future prospects for precise thermal management. Besides, as ferromagnets have recently been shown to be particularly suitable for active cooling applications [59], interconnected metal NW networks offer good application prospects in this field. On this basis, the present work also contributes to the emergence of flexible thermoelectric materials and devices to address the rapid development of miniature, lightweight and functional portable electronic devices [30]. It should be noted that similar magnetic thermoelectric switches can be obtained by other combinations of materials. Moreover, the material composition of the thermoelectric legs can be adjusted to allow the device to operate at the desired temperature [24]. A similar approach has also been used to develop a thermoelectric generator device that switches the sign of the thermoelectric voltage under the application of a magnetic field [24].

4. Conclusion and perspectives

Direct electrodeposition within track-etched PC template with crossed nanopores have been proved to be a cheap, versatile and suitable technique for the fabrication of large-area, robust and flexible 3D CNW networks embedded in polymer matrix. The technique allows a control over a wide range of parameters such as the network geometry, the NW diameter and packing factor, as well as their material composition and morphology. The 3D structure allows for easy electric and thermoelectric measurements with the electrical/thermal current applied in the macroscopic IP direction of the composite film, while being locally restricted along the NW axis. This approach is expected to optimize the output power of the nanowire based thermoelectric device.

CNW networks made of ferromagnetic metals and alloys have been found to display large thermoelectric power factors, which are only slightly smaller than the high power factors exhibited by their bulk constituents. Moreover, both *p*-type and *n*-type thermoelectric materials have been obtained, which is of paramount importance for the development of practical thermoelectric devices made of a succession of *p*-*n* thermocouples connected electrically in series and thermally in parallel. Such device can be deposited within a single flexible PC template, with desired shapes and sizes. The flexibility and shapeability of the films make them promising systems to harvest waste heat on surface with complex geometry or even the human body. Besides, the flexibility of CNW devices increases their durability under repeated bending or stretching. Other advantages of these metallic CNW structure are the low toxicity of the constituent materials and their light weight.

It has been found that the thermoelectric power of FM/Cu multilayer nanowires is only slightly reduced compared to that of ferromagnetic metals alone when the layer thicknesses of the ferromagnet and normal metal are comparable. Therefore, FM/Cu multilayers combine high thermoelectric power factors and giant magneto-transport effects. Giant magnetoresistance and magneto-Seebeck effects were obtained in FM/Cu CNW networks, up to 30% at RT for the $Co_{50}Ni_{50}$/Cu system. Besides, large magnetic variation of the thermoelectric power $\Delta S = S_0 - S_{sat}$ of about 5.5 μV K^{-1} and 5.1 μV K^{-1} were observed at RT in $Co_{50}Ni_{50}$/Cu an Py/Cu CNWs, respectively.

A new concept of thermoelectric magnetic switch, obtained from a thermocouple film whose legs are formed of homogeneous Co_3Ni_{97} CNWs and multilayer CNWs ($Co_{50}Ni_{50}$/Cu or Py/Cu) has been demonstrated, where a switching of the thermoelectric voltage between zero and a few tens of μV can be achieved when the external magnetic field is turned on or off. These flexible thermoelectric switches show promise for logic computing and sensors powered by waste heat. In addition, Onsager reciprocity between Peltier and Seebeck effects implies that a switchable Seebeck voltage results in a switchable Peltier heat flow. Therefore, the flexible thermoelectric modules developed here can be used as thermal switches, offering future prospects for precise thermal management, as ferromagnetic CNW have recently been shown to be particularly suitable for active cooling applications. However, challenges lie in the high resistance usually displayed by CNW networks along the IP direction, resulting in large Joule heating. Therefore, future developments of magneto-thermoelectric devices for heat management using 3D interconnected nanowire network will aim to reduce the electrical resistance by adjusting the dimensions, notably by taking advantage of an out-of-plane application of the heat gradient or Peltier current. Indeed, in this configuration, much lower resistances are expected for crossed nanowire networks.

However, the contact resistances inherent in this geometry can be a barrier to device development.

The versatility of the manufacturing process for such flexible thermoelectric devices allows the requirements of various specific applications to be met. Moreover, the fabrication of similar interconnected NW networks made of Bi alloys might lead to flexible thermoelectric modules with high figure of merit, although several additional fabrication challenges arise from the precise control of the crystal microstructure that is required to achieve high thermoelectric conversion efficiency in these materials [4, 6, 10].

Data availability statement

The data that support the findings of this study are available upon reasonable request from the authors.

Acknowledgments

N M acknowledges the Research Science Foundation of Belgium (FRS-FNRS) for financial support (FRIA Grant). F A A is a Postdoctoral Researcher of the FNRS. The authors would like to thank Dr E Ferain and the it4ip Company for supplying polycarbonate membranes. Financial support was provided by Wallonia/Brussels Community (ARC 18/23-093) and the Belgian Fund for Scientific Research (FNRS).

ORCID iDs

Tristan da Câmara Santa Clara Gomes https://orcid.org/0000-0002-5214-0377
Nicolas Marchal https://orcid.org/0000-0001-8150-7214
Flavio Abreu Araujo https://orcid.org/0000-0001-7157-3197
Luc Piraux https://orcid.org/0000-0003-0684-4338

References

[1] Hicks L D and Dresselhaus M S 1993 *Phys. Rev.* B **47** 12727–31
[2] Chen G, Dresselhaus M S, Dresselhaus G, Fleurial J P and Caillat T 2003 *Int. Mater. Rev.* **48** 45–66
[3] Mingo N 2004 *Appl. Phys. Lett.* **84** 2652–4
[4] Hochbaum A I, Chen R, Delgado R D, Liang W, Garnett E C, Najarian M, Majumdar A and Yang P 2008 *Nature* **451** 163–7
[5] Boukai A I, Bunimovich Y, Tahir-Kheli J, Yu J K, Goddard W A III and Heath J R 2008 *Nature* **451** 168–71
[6] Lin Y M, Sun X and Dresselhaus M S 2000 *Phys. Rev.* B **62** 4610–23
[7] Lin Y M, Cronin S B, Ying J Y, Dresselhaus M S and Heremans J P 2000 *Appl. Phys. Lett.* **76** 3944–6
[8] Zhou J, Jin C, Seol J H, Li X and Shi L 2005 *Appl. Phys. Lett.* **87** 133109
[9] Zhang G, Fang H, Yang H, Jauregui L A, Chen Y P and Wu Y 2012 *Nano Lett.* **12** 3627–33
[10] Hamdou B, Kimling J, Dorn A, Pippel E, Rostek R, Woias P and Nielsch K 2013 *Adv. Mater.* **25** 239–44
[11] Blatt F J, Schroeder P A, Foiles C L and Greig D 1976 *Thermoelectric Power of Metals* (Boston, MA: Springer)
[12] Watzman S J, Duine R A, Tserkovnyak Y, Boona S R, Jin H, Prakash A, Zheng Y and Heremans J P 2016 *Phys. Rev.* B **94** 144407
[13] Vandaele K, Watzman S J, Flebus B, Prakash A, Zheng Y, Boona S R and Heremans J P 2017 *Mater. Today Phys.* **1** 39–49
[14] Zebarjadi M 2015 *Appl. Phys. Lett.* **106** 203506
[15] Adams M, Verosky M, Zebarjadi M and Heremans J 2019 *Phys. Rev. Appl.* **11** 054008
[16] Chen Y, He M, Liu B, Bazan G C, Zhou J and Liang Z 2017 *Adv. Mater.* **29** 1604752
[17] Böhnert T, Vega V, Michel A K, Prida V M and Nielsch K 2013 *Appl. Phys. Lett.* **103** 092407
[18] Niemann A C *et al* 2016 *Adv. Electron. Mater.* **2** 1600058
[19] Böhnert T *et al* 2014 *Phys. Rev.* B **90** 165416
[20] Gravier L, Fábián A, Rudolf A, Cachin A, Wegrowe J E and Ansermet J P 2004 *J. Magn. Magn. Mater.* **271** 153–8
[21] da Câmara Santa Clara Gomes T and Piraux L 2019 *Sci. Adv.* **5** eaav2782
[22] Abreu Araujo F, da Câmara Santa Clara Gomes T and Piraux L 2019 *Adv. Electron. Mater.* **5** 1800819
[23] Marchal N, da Câmara Santa Clara Gomes T, Abreu Araujo F and Piraux L 2020 *Nanoscale Res. Lett.* **15** 137
[24] da Câmara Santa Clara Gomes T, Marchal N, Abreu Araujo F and Piraux L 2021 *Adv. Mater. Technol.* **n/a** 2101043
[25] Lee S F, Pratt W P, Loloee R, Schroeder P A and Bass J 1992 *Phys. Rev.* B **46** 548–51
[26] Bass J 2016 *J. Magn. Magn. Mater.* **408** 244–320
[27] Farrell T and Greig D 1970 *J. Phys. C: Solid State Phys.* **3** 138
[28] Cadeville M C and Roussel J 1971 *J. Phys. F: Met. Phys.* **1** 686
[29] da Câmara Santa Clara Gomes T, Marchal N, Abreu Araujo F and Piraux L 2020 *Nanomaterials* **10** 2092
[30] Fan Z, Zhang Y, Pan L, Ouyang J and Zhang Q 2021 *Renew. Sustain. Energy Rev.* **137** 110448
[31] Wang Y, Yang L, Shi X L, Shi X, Chen L, Dargusch M S, Zou J and Chen Z G 2019 *Adv. Mater.* **31** 1807916
[32] Zhang L, Shi X L, Yang Y L and Chen Z G 2021 *Mater. Today* **46** 62–108
[33] Bahk J H, Fang H, Yazawa K and Shakouri A 2015 *J. Mater. Chem.* C **3** 10362–74
[34] Du Y, Xu J, Paul B and Eklund P 2018 *Appl. Mater. Today* **12** 366–88
[35] Piraux L, da Câmara Santa Clara Gomes T, Abreu Araujo F and de la Torre Medina J 2020 3D magnetic nanowire networks *Magnetic Nano- and Microwires* 2nd edn, ed M Vázquez (Amsterdam: Elsevier) ch 27
[36] Ferain E and Legras R 2003 *Nucl. Instrum. Methods Phys. Res.* B **208** 115–22
[37] Rauber M, Alber I, Müller S, Neumann R, Picht O, Roth C, Schökel A, Toimil-Molares M E and Ensinger W 2011 *Nano Lett.* **11** 2304–10
[38] Araujo E, Encinas A, Velázquez-Galván Y, Martinez-Huerta J M, Hamoir G, Ferain E and Piraux L 2015 *Nanoscale* **7** 1485–90
[39] da Câmara Santa Clara Gomes T, de la Torre Medina J, Velázquez-Galván Y, Martínez-Huerta J M, Encinas A and Piraux L 2016 *J. Appl. Phys.* **120** 043904
[40] da Câmara Santa Clara Gomes T, Lemaitre M and Piraux L 2016 *Nanoscale Res. Lett.* **11** 466
[41] Velázquez Galván Y G, Santa Clara Gomes T, Piraux L and de la Torre Medina J 2020 *J. Magn. Magn. Mater.* **503** 166615
[42] Santa Clara Gomes T, Marchal N, Abreu Araujo F and Piraux L 2019 *Appl. Phys. Lett.* **115** 242402

[43] da Câmara Santa Clara Gomes T, Marchal N, Abreu Araujo F, Velázquez Galván Y, de la Torre Medina J and Piraux L 2021 *Nanomaterials* **11** 221
[44] de la Torre Medina J, Darques M, Encinas A and Piraux L 2008 *Phys. Status Solidi* a **205** 1813–6
[45] Santa Clara Gomes T, Medina J D L T, Velázquez-Galván Y G, Martínez-Huerta J M, Encinas A and Piraux L 2017 *IEEE Trans. Magn.* **53** 2301006
[46] Marchal N, da Câmara Santa Clara Gomes T, Abreu Araujo F and Piraux L 2021 *Nanomaterials* **11** 1133
[47] Kamalakar M V and Raychaudhuri A K 2009 *Phys. Rev.* B **79** 205417
[48] Bubnova O, Khan Z U, Malti A, Braun S, Fahlman M, Berggren M and Crispin X 2011 *Nat. Mater.* **10** 429
[49] Kim S I *et al* 2015 *Science* **348** 109–14
[50] MacDonald D K C 1962 *Thermoelectricity: An Introduction to the Principles* (New York: Wiley)
[51] Rowe D M 1995 *CRC Handbook of Thermoelectrics* (Boca Raton, FL: CRC Press)
[52] Meaden G T 1965 *Electrical Resistance of Metals* (Berlin: Springer)
[53] Basargin O V and Zarkhov A I 1974 *Fiz. Met. Metalloved.* **37** 891–4
[54] Mayadas A F, Janak J F and Gangulee A 1974 *J. Appl. Phys.* **45** 2780–1
[55] Ho C, Chi T, Bogaard R, Havill T and James H 1981 Thermoelectric power of selected metals and binary alloy systems *Thermal Conductivity 17—Proc. 17th Int. Thermal Conductivity Conf. (Gaithersburg, Maryland)* (New York: Plenum Press) pp 195–205
[56] Shi J, Parkin S S P, Xing L and Salamon M B 1993 *J. Magn. Magn. Mater.* **125** L251–6
[57] Shi J, Kita E, Xing L and Salamon M B 1993 *Phys. Rev.* B **48** 16119–22
[58] Piraux L, George J M, Despres J F, Leroy C, Ferain E, Legras R, Ounadjela K and Fert A 1994 *Appl. Phys. Lett.* **65** 2484–6
[59] Adams M, Verosky M, Zebarjadi M and Heremans J 2019 *Phys. Rev. Appl.* **11** 054008